Surface Science 110 (1981) 19–42
North-Holland Publishing Company

THE STRUCTURE OF EPITAXIALLY GROWN METAL FILMS ON SINGLE CRYSTAL SURFACES OF OTHER METALS: GOLD ON Pt(100) AND PLATINUM ON Au(100)

J.W.A. SACHTLER, M.A. VAN HOVE, J.P. BIBÉRIAN * and G.A. SOMORJAI
Materials and Molecular Research Division, Lawrence Berkeley Laboratory, and Department of Chemistry, University of California, Berkeley, California 94720, USA

Received 18 February 1981, accepted for publication 23 April 1981

Gold was evaporated onto Pt(100) and platinum was evaporated onto a Au(100) single crystal surface. Deposition of gold onto Pt(100) removed the $\left(\begin{smallmatrix}14 & 1\\ 1 & 5\end{smallmatrix}\right)$ reconstructed surface structure and at a coverage of about 0.5 monolayer a (1 × 1) pattern fully developed. This pattern remained unchanged up to 2 gold monolayers. Multilayers of gold produced (1 × 5) and (1 × 7) surface structures after annealing. These observations imply variable interatomic distances in the gold layers. The (1 × 5) and (1 × 7) surface structures can be explained by the formation of a hexagonal top atomic layer on a substrate that retains a square lattice. The well known structure of clean Au(100) did not form, even at 32 layers of gold on Pt(100). Platinum deposited onto Au(100) removed its surface reconstruction yielding a fully developed (1 × 1) pattern at about one-half layer. This pattern remained unchanged upon further platinum deposition. The absence of new reconstructions in this case may be linked with the growth mechanism that is inferred from the variation of the Auger signal intensities of the substrate and adsorbate metals with coverage of the adsorbate. It was found that platinum on Au(100) forms microcrystallites (Volmer–Weber type growth), while gold on Pt(100) grows layer-by-layer (Frank–van der Merwe growth mechanism).

1. Introduction

Epitaxial systems composed of one metal deposited on the surface of another metal are important for several reasons. Metal coatings passivate surfaces aginst corrosion and radiation damage. Surfaces may be prepared this way with specific optical or electrical properties due to changes of absorbance and work function. They can also exhibit unique catalytic activity which is the reason for our interest in these systems. Bimetallic catalysts (Pt–Re [1–6], Pt–Ir [7,8], Pt–Sn [9], Pt–Au [10–13], Ni–Cu [14,15]) have marked selectivity, often higher specific rates (turnover frequencies) and greater resistance to poisoning than one-component metal catalyst systems.

* Permanent address: Laboratoire Surfaces–Interfaces, ERA, CNRS 070899, Faculté des Sciences de Luminy, F-13288 Marseille Cédex 2, France.

0039-6028/81/0000–0000/$02.50

The surface structures of many such metal-on-metal systems have been reviewed recently [16]. These data indicate the predominance of the adsorbate–substrate interaction in determining order at low coverages where the adsorbate and substrate surface structures are closely related. At higher coverages more complex ordering characteristics were found.

In this paper we report a study of the surface structures of a new combination of metals with unique structural and catalytic properties, viz. the gold–platinum system. Gold was deposited by evaporation onto a Pt(100) single crystal surface and conversely platinum was vapor-deposited onto Au(100). These surfaces were chosen for our studies because in both cases the clean substrate surfaces are reconstructed in a similar way. It was thought that changes in the substrate surface reconstruction during the deposition of the other metal could provide additional information about the nature of the surface structures that form in these epitaxial metal-adsorbed-on-metal systems.

In our experiments with Au on Pt(100) and Pt on Au(100) we found that the deposited metal removed the clean surface reconstruction and that structures were formed that had either a square or a hexagonal atomic arrangement in the top layer. As the deposited layer varied in the thickness up to many layers, low energy electron diffraction (LEED) patterns were observed that could be explained by assuming variable bond lengths between the surface atoms. The Au on Pt(100) case appears to yield a greater variety of ordered surface structures than the Pt on Au(100) system. This may be linked with the adlayer growth mechanism, which is inferred from the variation of the Auger signal intensities of the substrate and adsorbate metals with coverage of the adsorbate. The growth mechanism determined for Au on Pt(100) is of the layer-by-layer type (Frank–van der Merwe type growth) while Pt deposited on a Au(100) single crystal surface formed three-dimensional crystallites (Volmer–Weber growth mechanism).

2. Experimental

The experiments were carried out in an ultrahigh vacuum (UHV) system equipped with LEED, Auger electron spectroscopy (AES), and a quartz crystal thickness monitor (QXTM). The four-grid LEED optics were used to obtain diffraction patterns at various stages of the metal film growth. From the patterns the surface unit cell sizes and orientations could be determined as long as the deposit was ordered. We have not utilized the diffraction beam intensities for surface structure determination. Auger electrons were excited by a glancing incidence electron gun producing a primary electron beam with an energy of 2 keV and energy analyzed by the LEED optics. The platinum and gold single crystals were prepared by spark erosion of thin wafers from the corresponding high purity single crystalline rod (within 1° of the (100) face as determined by Laue X-ray back-diffraction). These wafers were polished mechanically before mounting in the vacuum chamber. The

Pt(100) crystals were cleaned in the vacuum chamber by argon ion sputtering followed by annealing at 1325 K and oxygen treatment at the same temperature to remove residual carbon. The Au(100) crystals were cleaned by argon ion sputtering and annealing at 875 K. After these treatments, the surfaces were clean, according to AES, and produced LEED patterns with sharp diffraction spots.

Gold and platinum were evaporated from a source inside a differentially pumped side chamber. The metal vapor beam could be interrupted by means of a rotatable shutter. The distance between the substrate and the evaporation source was 10 cm; the metal single crystal was rotated between the positions used for deposition, AES, and LEED analysis. The QXTM was mounted on bellows to enable both measurement of the deposition rate and, by moving the QXTM away, subsequent deposition onto the metal single crystal surface at the same position. In this way there was no difference in the metal vapor fluxes received by the metal crystal and the thickness monitor. The QXTM provided independent measurement of the rate of metal deposition which was used together with AES for the determination of surface compositions. In this way coverages could be determined with an accuracy of within 10%. The coverages that were determined with the QXTM are by nature an average over the crystal surface and may be expressed as monolayer equivalents, i.e. the number of monolayers that the deposited metal would have formed if it had grown layer-by-layer. This number is equal to the ratio of the number of deposited

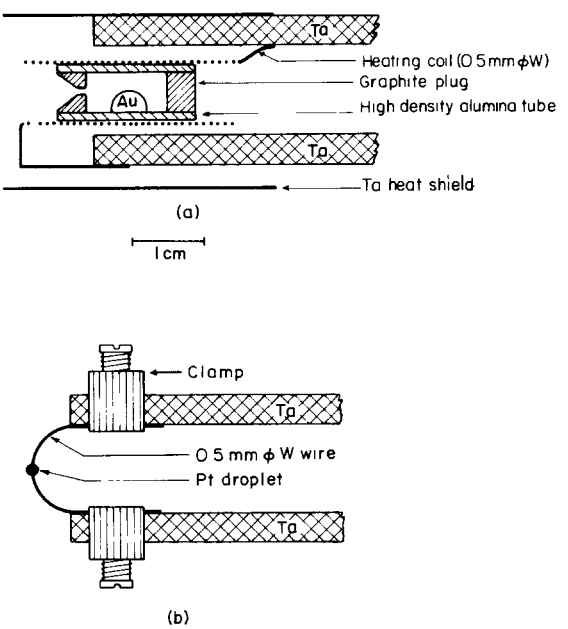

Fig. 1. Schematic representation of the evaporation sources for gold and platinum: (a) effusive type source used for the evaporation of gold; (b) platinum source.

atoms and the number of substrate surface atoms.

Two different kinds of evaporation sources were used for gold and for platinum. Gold was evaporated from an effusive type source, schematically shown in fig. 1a. With this arrangement the deposition rate (as measured at the substrate) could be varied easily Typically, this rate was tuned to about 12 layers of gold per hour.

An effusive source cannot readily be made for the evaporation of platinum because of the much higher temperatures needed to obtain a sufficiently large metal vapor flux. Platinum was evaporated from a tungsten wire, as shown in fig. 1b. A platinum droplet was formed by melting a piece of 0.5 mm diameter platinum wire that was wrapped around the 0.5 mm diameter tungsten wire, in vacuum. With this evaporation source, deposition rates were typically around one layer per hour. Sometimes the rate could be increased to about three layers per hour, but this generally reduced the lifetime of the platinum source. The surface compositions were determined by AES in conjunction with the QXTM. The Auger spectra of platinum and gold that were to be used for determination of the growth mechanism were recorded in the energy range of 45–95 eV using a modulation of 2 V peak-to-peak. The quantitative analysis of these spectra is described in the appendix.

3. Results

3.1. Gold on Pt(100)

3.1.1. LEED observations

In our experiments we start with the clean Pt(100) surface that exhibits the usual $(^{14}_{1}\ ^{1}_{5})$ reconstruction [17]. As Au is deposited onto this surface at 300 K, the extra spots due to the reconstruction gradually weaken, leaving a fully developed (1 × 1) pattern at a gold coverage of 0.5 monolayer, c.f. fig. 2. (The gold coverage can be expressed in monolayers since Au on Pt(100) grows through a layer-by-layer mechanism as will be shown later in this paper.) This pattern remains unchanged up to two monolayers of gold. A five minute anneal of one monolayer of Au on Pt(100) at 1075 K generates a faint (20 × 5) like pattern in addition to the (1 × 1) pattern, while the Au Auger signal decreases, indicating platinum diffusion to the surface. Around 2 monolayers of gold annealing at 675 K adds to the sharp (1 × 1) pattern very faint streaks linking neighbouring (1 × 1) spots in [011] directions (these are the directions in which 5th order spots can occur). Annealing at high temperatures will again eventually give rise to a (20 × 5) like pattern. With three gold layers, the as-deposited Au produces similar, but more intense streaks. Annealing at 675–875 K produces a well-defined (1 × 7) pattern that changes into a (1 × 1) pattern with faint streaks after heating to 975 K. There is a small decrease in the gold Auger signal at this stage. For 21 gold layers, the as-deposited structure is the same as with three gold layers (fig. 2). Annealing at 625–975 K now first produces a fuzzy (1 × 5) pattern, which develops into a (1 × 7) pattern upon annealing at 1025–

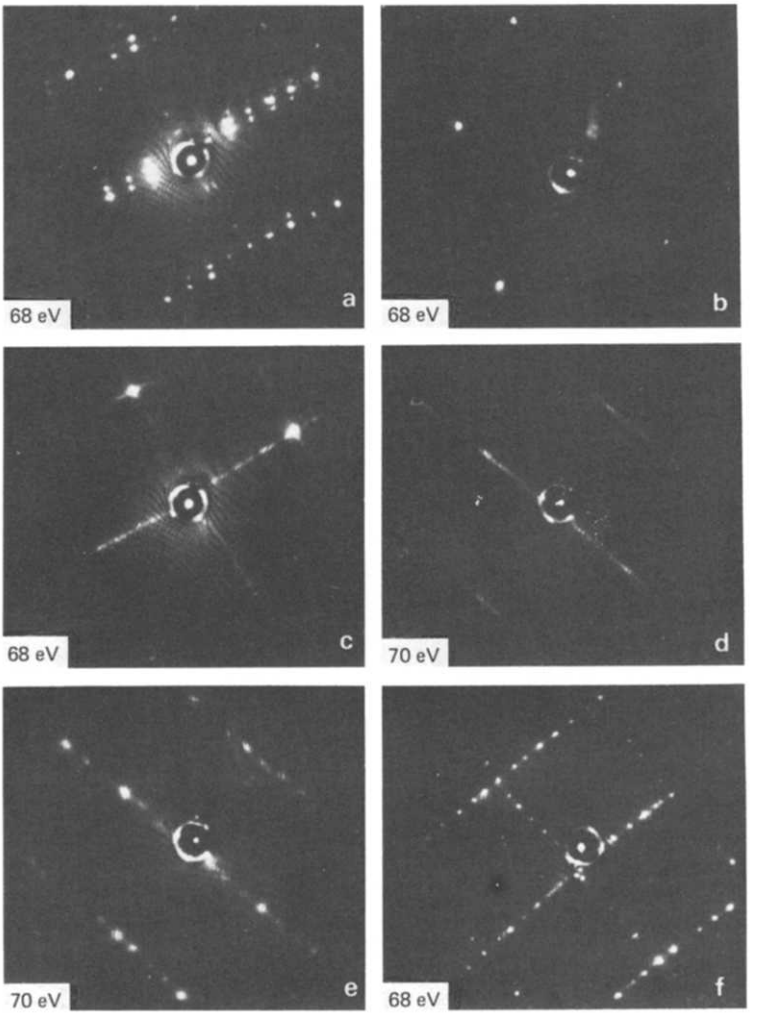

Fig. 2. LEED patterns observed for Au on Pt(100) at various gold coverages and after different heat treatments; the surfaces were prepared at 300 K unless annealing temperature is indicated. (a) Clean Pt(100), (b) 0.5 monolayer Au; (c) 2.5 layers Au, (d) 32 layers Au; (e) 32 layers Au, 923 K, (f) 21 layers Au, 1023 K.

1175 K, c.f. fig. 2. A 32 layer thick gold deposit starts out with the same surface structure as 3 or 21 monolayers. Annealing to 625–925 K yields a better defined, though still somewhat streaked and fuzzy (1 × 5) pattern (fig 2). Further annealing at 925 K again produces the sharp (1 × 7) pattern, while prolonged (10 min) heating at 1175 K gives rise to a (1 × 1) pattern. At this time the Auger spectrum

Table 1
Bond length expansions in Au layers deposited on Pt(100)

	Number of Au layers on Pt(100)		0–2	3	3	3	20–30	20–30	20–30	20–30
	Anneal temperature (K)		Any	None	675	975	None	<1025	1025	1175
	Pattern		(1 × 1)	Streaked	(1 × 7)	(1 × 1)	Streaked	Fuzzy (1 × 5)	(1 × 7)	(1 × 1)
(a)	Expansion (%)	// 5-fold direction	−4	−2	−3	−4	−2	−1 5	−3	−4
	2nd layer to bulk Au	⊥ 5-fold direction	−4	−2	−3	−4	−2	−1 5	−3	−4
(b)	Expansion (%)	// 5-fold direction	0	?	1	0	?	−4	1	0
	1st to 2nd layer	⊥ 5-fold direction	0	0	0	0	0	0	0	0
(c)	Same as (b) buckled	// 5-fold direction	0	?	3 5	0	?	−1.5	3.5	0
		⊥ 5-fold direction	0	0	0	0	0	0	0	0
(d)	Expansion (%)	// 5-fold direction	−4	?	−2	−4	?	−5.5	−2	−4
	1st layer to bulk Au	⊥ 5-fold direction	−4	−2	−3	−4	−2	−1 5	−3	−4
(e)	Same as (d) buckled	// 5-fold direction	−4	?	0.5	−4	?	−3	0 5	−4
		⊥ 5-fold direction	−4	−2	−3	−4	−2	−1.5	−3	−4

The bulk Au–Au bond length is used as reference For comparison the bulk Pt–Pt bond length is about 4% smaller than the bulk Au–Au distance By "5-fold direction" is meant the direction of the long side of the (1 × 5) or (1 × 7) unit cell, which is also the direction of streaking See text for further explanations

reveals the presence of some platinum which has diffused from the substrate through the gold to the surface.

As the epitaxial gold layers grow on Pt(100), the spot or streak positions can be monitored with enough precision to detect changes in the interatomic distances parallel to the surface in the first few layers. The basic (1 X 1) square of the diffraction pattern corresponds to the square lattice of the second layer (counted from the surface) and to a lesser extent of the deeper layers as well as well. The varying

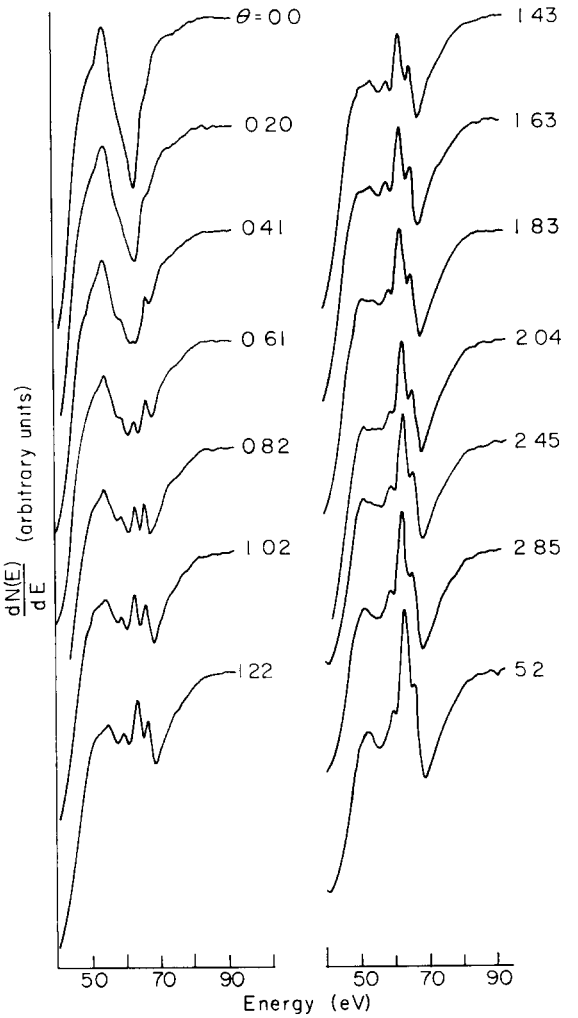

Fig. 3. Auger spectra of Au on Pt(100) at various gold coverages indicated by θ and expressed in monolayer equivalents.

dimension of this basic (1 X 1) square, transformed from reciprocal space to real space, is shown in the first row (row a) of table 1 where the bulk Au–Au distance is used as reference. The gold interatomic distance is clearly reduced when gold is deposited epitaxially onto the Pt(100) surface. It should be noted that despite this variation, the second layer always retains a square rather than rectangular lattice (within our precision of measurement of better than 1% of a bond length). This basic (1 X 1) square provides us with a calibration to determine the interatomic distances, parallel to the surface, within the topmost layer, as will be discussed in section 4.

3.1.2. AES observations

Platinum and gold are neighbors in the periodic table and their Auger spectra are very similar. The Auger energy range that is most suitable for analysis of the respective surface concentrations is between about 45 and 90 eV. Here the peak shapes of the Auger transitions change in a marked way during the deposition of gold on platinum as is shown in fig. 3. Also in this energy range the mean free path of the Auger electrons is small, which makes this part of the Auger spectrum most surface sensitive. The reason for the observed change in the peak shapes is the interference of the relatively broad 64 eV platinum peak with the 56, 61, 66, and 69 eV gold transitions. In order to extract the desired surface concentrations from these Auger spectra, separation of the gold and platinum peaks is necessary. The procedure for this decomposition is described in the appendix. The resulting normalized intensities of gold and platinum are plotted as a function of gold coverage in fig. 4. The

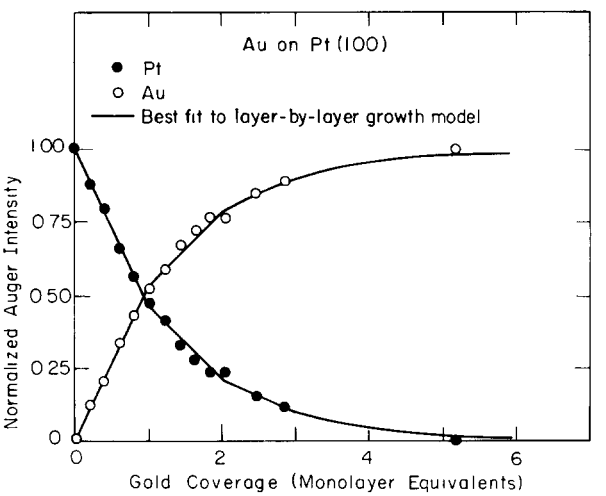

Fig. 4. Plot of the Auger intensities of gold and platinum after decomposition, versus gold coverage on Pt(100). The gold coverages were obtained with the QXTM

first breaks in the slopes of the curves in fig. 4, which are indicative of the completion of the first gold monolayer (c.f. discussion in section 4), occur at a coverage that agrees very well with the deposition of the first monolayer equivalent according to the QXTM. For comparison, fig. 4 also shows as solid lines the best fit that was obtained assuming a layer-by-layer (Frank–van der Merwe) growth mechanism.

Once this calibration has been performed any gold coverage between zero and about three layers can be determined simply by comparing the shape of its Auger spectrum in the 45–90 eV range with the reference spectra of known coverages, shown in fig, 3.

3.2. Platinum on Au(100)

3.2.1. LEED observations

The clean Au(100) single crystal surface shows the usual (20 × 5) LEED structure that is characteristic of this reconstructed surface. Deposition of platinum removes this reconstruction yielding a (1 × 1) pattern at a coverage of about one-half monolayer equivalent. This diffraction pattern does not change upon further platinum deposition, c.f. fig. 5. The LEED pattern of the reconstructed Pt(100) single crystal surface has not been observed for the platinum deposits on the Au(100) surface up to the highest coverage achieved in these experiments of eight monolayer equivalents. Annealing of these surfaces at temperatures up to 425–475 K does not change the LEED patterns, while heating to higher temperatures results in the loss of platinum due to diffusion into the gold crystal. Measurement of the distances between diffraction spots in the LEED patterns gives the same spot–spot distance for all these surfaces, regardless of the platinum coverage, namely the spot–spot distance characteristic of the gold bulk.

3.2.2. AES observations

The procedure followed for the quantitative Auger analysis of the surface com-

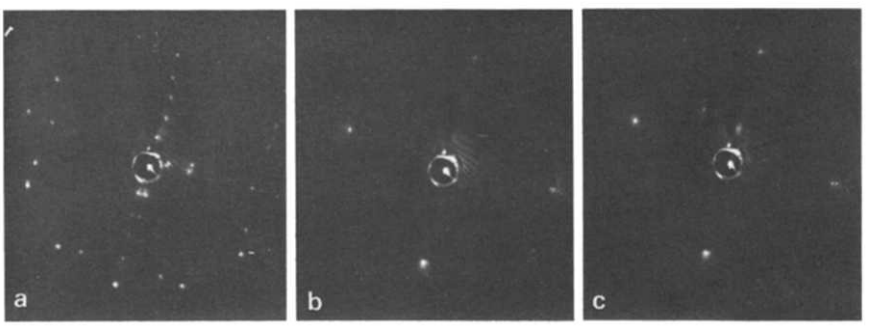

Fig. 5. LEED patterns observed at 51.5 eV for Pt on Au(100) at various platinum coverages (a) clean Au(100); (b) 1 mle Pt; (c) 2 mle Pt (mle = monolayer equivalent).

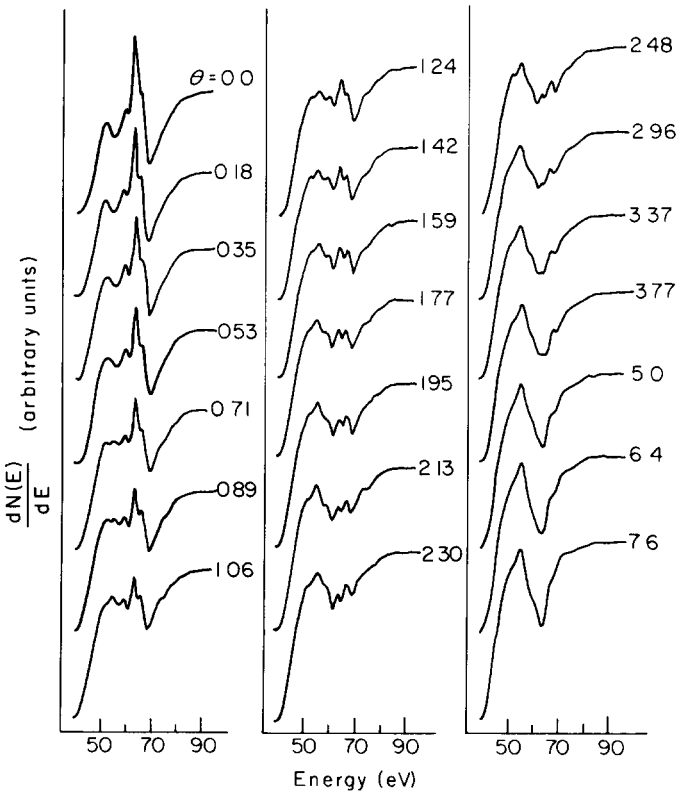

Fig 6. Auger spectra of Pt on Au(100) at various platinum coverages indicated by θ and expressed in monolayer equivalents

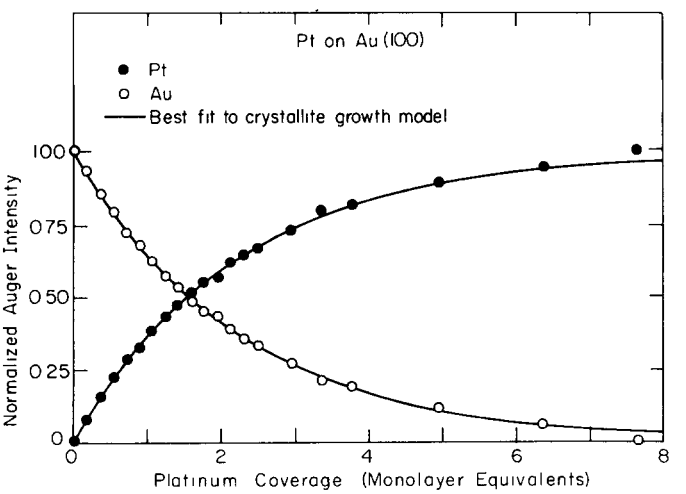

Fig. 7 Plot of the Auger intensities of gold and platinum after decomposition versus platinum coverage on Au(100). The platinum coverages were obtained with the QXTM.

position is the same as described in the appendix for gold on Pt(100). Again a series of Auger spectra was recorded at various platinum coverages (fig. 6). The normalized Auger intensities, after decomposition, of the platinum and gold Auger peaks are plotted as a function of the platinum coverage that was obtained using the QXTM in fig. 7. In this case no breaks in the curves are apparent. For comparison, fig. 7 also shows as solid lines the best fit that was obtained assuming a crystallite growth mechanism (Volmer–Weber type growth).

4. Discussion

4.1. Quantitative analysis of the AES observations

The procedure that was followed for the analysis is described in the appendix. As is shown there, two types of information can be obtained. First, from the variation of the Auger signal intensities of gold and platinum with coverage of the adsorbate metal (figs. 4 and 7), the growth mechanism of the deposited metal can be inferred. Second, also the mean free path of the Auger electrons, λ, can be derived. This parameter λ is related to the Auger signal intensity of one monolayer of material relative to the bulk intensity, $I(1)/I(\infty)$. (See eq. (6) in the appendix.)

Optimization of the fits of the data for Au on Pt(100) (fig. 4) with the various growth models (see appendix) yielded the following results: The best fit with the Frank–van der Merwe (FM) growth model gave a value of $I(1)/I(\infty) = 0.54$ (corresponding to $\lambda = 3.4$ Å).

This fit had a variance (i.e. sum of squares of the differences between calculated and experimental points) $V = 0.0034$. Fitting the crystallite growth model that uses the Poisson distribution to these data yielded $I(1)/I(\infty) = 0.73$ ($\lambda = 2.0$ Å) with $V = 0.0061$. It may be noted that according to the Poisson distribution after deposition of one mle (monolayer equivalent) actually only 37% of the platinum is covered by gold. The variances indicate that the FM growth model is preferred. This is also supported by the resulting $I(1)/I(\infty)$ values, as an $I(1)/I(\infty) = 0.73$ seems unreasonably high, or the corresponding electron mean free path of only 2.0 Å too short. In the coverage range of up to about one mle of gold the data could also be fit with the crystallite growth model that represented the particle shapes as identical hemispheres (ih). This fit that yielded $I(1)/I(\infty) = 0.62$ was as good as the one with the FM model and also better than with the Poisson distribution in this coverage range. Inspection of this result reveals that at a coverage of one mle actually 70% of the Pt substrate is covered with gold. However, when the ih model was tested on a theoretical ASc plot that was generated for layer-by-layer growth, a similar effective coverage was found which indicates that this model is not able to reproduce the FM type growth accurately. The low variance that was found indicates that the first part of the ASc plot is not sensitive to small details of the growth mechanism. These differences do become more apparent when larger parts of the ASc plot are

used for the fitting. Unfortunately, the ih model cannot be calculated beyond about one mle as the crystallites will touch each other and it is not clear what happens at this point.

When a growth mechanism operates that resembles layer-by-layer growth but in which the second layer forms before the first monolayer has become "perfect", completely free of defects, an ASc plot will result in which the coverage dependence of the Auger signal intensities is weakened. Thus the curve for the substrate will lie above that of the perfect FM type growth and conversely the curve for the adsorbate will be below the curve of perfect layer growth. These deviations will be larger when the concentration of defects is larger and they will be more apparent at higher coverages. As can be seen in fig 4, the experimental data fit the "perfect" layer growth model very well, even at high coverages and thus the defect concentration should be small. It is difficult, however, to express this more quantitatively. It is estimated that a defect concentration of the first mle of 10–20% would probably be difficult to detect.

The Stranski–Krastanov (SK) growth model can be rejected using similar arguments. For the first monolayer the ASc plot for this model is identical to that of the FM type growth. At coverages exceeding the first monolayer crystallite growth should occur, and the ASc plot should have curves that show a much weaker coverage dependence than those of layer-by-layer growth. As can be seen in fig. 4, the experimental points do not show this deviation from the solid lines that represent the FM model, even at high coverages.

In conclusion, the experimental results in fig 4 were best fit with the layer-by-layer or Frank–van der Merwe growth mechanism, which yielded $I(1)/I(\infty) = 0.54 \pm 0.05$ which corresponds to $\lambda = 3.4 \pm 0.5$ Å. It may be, however, that the layer growth is less than perfect, i.e. the second layer begins to form somewhat before the first monolayer has been fully completed.

In the case of Pt on Au(100) fitting the data, shown in fig. 7, with the various growth models gave the following results. In the coverage range from 0 to 5 mle, the best fit with FM type growth gave $I(1)/I(\infty) = 0.37$, which corresponds to $\lambda = 6.0$ Å, with a variance $V = 0.0028$. Using the crystallite growth model with the Poisson distribution $I(1)/I(\infty) = 0.45$ ($\lambda = 4.6$ Å) and $V = 0.0007$ were obtained. Up to a coverage of 1.8 mle the data could also be fit with the ih model, yielding $I(1)/I(\infty) = 0.45$ ($\lambda = 4.6$ Å) and a concentration of nucleation sites $C^n = 0.06$. The latter corresponds to a crystallite separation of about 12 Å. The uncertainty in these two numbers is difficult to assess, however. In order to determine whether a Stranski–Krastanov (SK) growth mechanism could be operating, the data in fig. 7 were also fit only up to 1 mle. Here the FM model gave $I(1)/I(\infty) = 0.37$ and $V = 0\ 0014$, the crystallite growth with the Poisson distribution $I(1)/I(\infty) = 0.45$, and $V = 0.0002$ and the ih crystallite model $I(1)/I(\infty) = 0.45$, $V = 0.004$, and $C^n = 0.06$. If the SK were to operate the best fit should have been obtained with the layer-by-layer type growth which clearly is not the case.

In conclusion, the experimental data for Pt on Au(100) were best fit with a crys-

tallite or Volmer–Weber growth mechanism. In particular, the model that used a Poisson distribution to describe the particle shapes gave the best fit. This fit is shown as the solid lines in fig. 7. The resulting relative monolayer value is $I(1)/I(\infty) = 0.45 \pm 0.05$ which corresponds to $\lambda = 4.6 \pm 0.6$ Å.

By comparing figs. 4 and 7, the following qualitative observation can be made that strengthens the above conclusion. The dependence of the Auger signal intensity on the adsorbate coverages is the strongest for layer-by-layer growth, giving the most rapid decrease of the substrate signal and conversely the most rapid increase of the adsorbate Auger signal intensity with increasing coverage. When the adatoms aggregate to form three-dimensional crystallites this coverage dependence of the signal intensities becomes weaker; the bigger the aggregates are at a given coverage (and consequently the fewer are on the surface) the weaker this dependence will be. Comparing figs. 4 and 7 reveals the stronger coverage dependence for the former, i.e. the Au on Pt(100) system and the weaker dependence for the latter, i.e. the Pt on Au(100) system. This is in accordance with the growth mechanisms that were derived in the above sections.

These findings are easily understood as gold has a lower surface free energy than platinum (1.483 and 2.465 J m^{-2} at 300 K, respectively, calculated with the data from ref. [29]). When gold atoms cover the platinum substrate, the surface free energy of the system decreases. The largest decrease is obtained when the number of platinum atoms that becomes covered by a gold adatom is maximized. This is obviously the case when the deposited gold forms a monolayer. Conversely, the deposition of platinum onto Au(100) increases the surface free energy of the system. This increase will be smallest when the number of gold atoms that becomes covered by platinum is minimized. This can be achieved when the platinum atoms aggregate into three-dimensional clusters, thus leading to a crystallite growth mechanism.

The two values of $I(1)/I(\infty)$ for Au on Pt(100) and Pt on Au(100) are in good agreement with each other and also with literature values for Pt of $I(1)/I(\infty) = 0.51$ (for carbon on a stepped platinum surface Pt(S)–[6(111) × (100)] [18]), $I(1)/I(\infty) = 0.42$ (for Pt on Pd [19]), and $I(1)/I(\infty) = 0.47$ (for Pd on Pt [19] and Ir on Pt [20]).

4.2. Review of the clean Pt(100) and Au(100) surface structures

The clean Pt(100) and Au(100) single crystal surfaces reconstruct and have been investigated extensively [17,21,22]. The LEED observations of the reconstructions of these surfaces and also of the clean Ir(100) surface [17,23] can be explained within the framework of a hexagonally close packed surface layer resting on top of an atomic layer with a square lattice [17]. This is illustrated in fig. 8. The clean surface reconstructions of the (100) faces of Pt, Au, and Ir have longer been interpreted using this model on the basis of LEED patterns, photoemission data [24], and ion scattering measurements [25]. Recently a LEED intensity analysis has con-

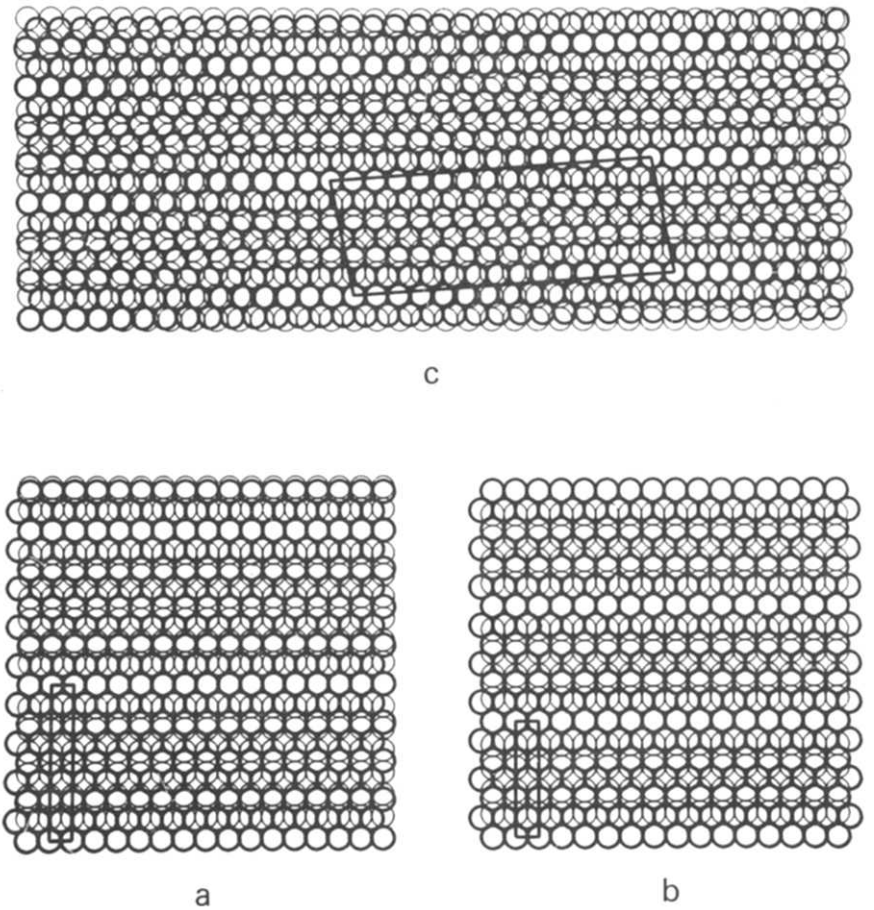

Fig. 8. Real space models of several surface reconstructions: (a) (1 × 7) structure, (b) (1 × 5) structure; (c) $(\begin{smallmatrix}14 & 1\\ 1 & 5\end{smallmatrix})$ structure.

firmed and refined this structure [17], showing that the hexagonal top layer buckels somewhat. This buckling absorbs part of the bond length contraction that must be assumed in the hexagonal layer to explain the observed LEED patterns. For example, the Ir(100) (1 × 5) structure requires a 4% uniaxial contraction if no buckling is allowed to achieve the (1 × 5) coincidence in the 5-fold direction. With the buckling found by the LEED intensity analysis, this contraction needs only to be about 1.5%. Similarly, for Pt(100) and Au(100), after correction for buckling, bond lengths parallel to the surface are found to contract by about 3% and 4%, respectively, this time not unaxially, but approximately isotropically in the surface. These larger contractions are deduced from the observed LEED patterns, $(\begin{smallmatrix}14 & 1\\ 1 & 5\end{smallmatrix})$ for

Pt(100) and approximately (20 × 5) for Au(100). The differences in bond length contraction between Ir, Pt, and Au(100) are thus partly deduced from the difference in the observed unit cells. It should be emphasized that the kind of pattern that is observed for a certain surface is characteristic only for the relative size of the first atomic layer with respect to the second atomic layer. The *absolute* size can be found, for example, by comparison of spot–spot distances in the diffraction patterns with spot–spot distances for known lattices. We shall make this absolute determination by comparing the size of the square reciprocal lattice of the second layer from the surface with that of the square reciprocal lattice of the clean Pt(100) substrate, whose lattice constant is known. These sizes are then expressed relative to clean Au(100) using the known lattice constants of 3.9239 Å for platinum and 4.0785 Å for gold [26].

4.3. Surface structure of Pt(100) covered by up to one monolayer of gold

Our AES measurements show that Au on Pt(100) grows layer-by-layer so that coverages can be expressed in true monolayers. The observation that approximately one half monolayer of Au on Pt(100) converts the $(\frac{14}{1}\ \frac{1}{5})$ clean surface reconstruction to a (1 × 1) structure is interesting in several respects. First, it confirms that the presence of a gold adlayer can remove the clean surface reconstruction. This surface restructuring can be interpreted as an increase in the bond lengths of the topmost Pt atoms that is large enough to render the hexagonal reconstruction unfavorable. Second, it shows that despite the available hexagonally reconstructed platinum surface, the adlayer chooses not to grow with its (111) axis perpendicular to the surface, unlike many other epitaxial metal-on-metal systems [16]. Another example of the former occurs for Au on Pd(100) which produces a (1 × 1) pattern corresponding to a 4.7% bond length contraction for the deposited Au [22]. Third, the Au–Au bonds in the monolayer on Pt(100) are now contracted by about 4% with respect to bulk Au–Au bonds in order to fit on the Pt(100) substrate. This contraction of 4% is to be compared with the 4% contraction observed for the clean Au(100) (20 × 5) reconstructed surface layer and with the 4.7% contraction reported for a Au monolayer on Pd(100) [22].

4.4. Surface structure of Au(100) covered by up to one monolayer equivalent of platinum

As platinum is deposited onto a Au(100) single crystal surface, the (20 × 5) reconstruction of the substrate disappears and at a platinum coverage of about one-half monolayer equivalent, a (1 × 1) pattern is fully developed. This is similar to the Au on Pt(100) case, except that our AES data indicate that platinum forms microcrystallites on the Au(100) single crystal surface (see section 4.1). These microcrystallites must be small compared to the coherence width of the electron beam (i.e. $\ll$100 Å) since no diffraction from facets is observed, which is also supported by

the fact that the (1 × 1) spots are broadened in the presence of the adsorbate layer. This conclusion is in accordance with the results from our Auger model calculations (which are described in the appendix) where, assuming that the platinum crystallites are growing as identical halfspheres, an optimal microcrystallite separation of about 12 Å was found (cf. section 4.1). These microcrystallites, therefore, most likely have only small (100) planes, which, even if they did reconstruct could not produce additional diffraction features due to lack of sufficiently large domain size. Measurement of spot–spot distances in the LEED patterns indicates that the platinum assumes the substrate, Au(100), lattice spacing. However, this is not certain since the platinum microcrystallites are much smaller than the coherence width of the LEED electron beam and the interpretation of LEED patterns is not well established under those conditions.

4.5. Surface structures of multilayers of gold on Pt(100)

As the gold monolayer coverage is exceeded the surface structure remains unchanged up to two monolayers. Deposition of more gold causes the appearance of streaks which remain up to 32 layers of gold, the highest coverage attained in our experiments. Annealing of these surfaces gives rise to the appearance of the (1 × 5) and (1 × 7) structures. These patterns are similar to the ones that have been found for Au on Pd(100) [22], although the conditions differ. On Pd(100) one monolayer of Au formed a (1 × 1) pattern, implying a 4.7% contracted bond length in the square Au lattice. For thicker deposits, streaked patterns occurred, interrupted by a (1 × 7) pattern at about 4 monolayers of Au on Pd(100), and finally a (1 × 5) pattern appeared at about 15 monolayers. In these experiments no annealing was necessary to obtain the reconstructed surfaces.

Using the same reasoning as with the clean surface reconstructions, interatomic distances in these surface structures can be obtained. For that purpose only one surface structure needs to be described in addition to those mentioned in section 4.2, namely the (1 × 7) structure. This can be obtained with a 1% expansion of the hexagonal layer in the 7-fold direction before buckling, or an expansion of about 3.5% after buckling with no change in the 1-fold direction.

The resulting variations in interatomic distances parallel to the surface of Au on Pt(100) are given in table 1. In row a we indicate, as described previously, the size relationship between the square second layer (the layer just below the outermost layer) and a bulk Au(100) layer, as derived from the measured spot–spot distances in photographs of LEED patterns. In row b, the size relationship between the first (i.e. topmost) layer and the second (i.e. next) layer is entered, based on the type of LEED pattern that is observed and assuming no buckling in the top layer. In row c a buckling correction amounting to 2.5% is added to the values of row b, assuming that the buckling is the same as was obtained in a detailed structural analysis of the Ir(100) (1 × 5) and Pt(100) $(^{14}_{1}\ ^{1}_{5})$ surface reconstructions. In row d of table 1 the size of the first (outermost) layer is related to that of the bulk gold by adding the

expansion percentages of rows a and b, thereby giving the absolute bond length change in the topmost layer. In row e the correction for buckling described above is added to the results of row d.

We would like to compare these results to previous observations, however, in the only directly comparable case, that of Au on Pd(100), no bond lengths are quoted for the thicker overlayers [22]. The (1 X 7) pattern was interpreted as due to a hexagonal Au overlayer, contracted by about 5%, lying on the square lattice Pd(100) substrate. Since Pd has a smaller lattice constant than Au, it is easy to see that a (1 X 7) unit cell is preferred over a (1 X 5) unit cell, in this case.

As mentioned before, the second layer from the surface appears to always retain a square lattice as opposed to a rectangular lattice, despite changing bond lengths in that layer. This indicates isotropic changes in the subsurface bond lengths parallel to the surface, whereas there is no isotropy in the changes occurring in the top (hexagonal) layer, the hexagon is distorted somewhat to fit in a (1 X 5) or (1 X 7) superlattice on the square layer beneath it. As indicated in table 1, with increasing thickness of the gold layer, the lattice constant of the subsurface layer tends toward bulk Au, however, without reaching it even at a total deposit thickness of 32 gold layers.

When the surfaces are annealed at high temperatures, Pt diffuses to the surface and a (1 X 1) LEED pattern is observed. The appearance of platinum in the surface layer reduces the bond lengths to those of one (1 X 1) monolayer of Au on Pt(100), which is identical to the Pt–Pt distances or 4% contracted bond lengths with respect to bulk gold. The surface concentration of platinum that is needed to bring about the (1 X 1) structure cannot be determined in our experiments since the concentration depth profile, after diffusion of platinum through gold (and vice versa), is not known.

The bond length variations observed in the epitaxial layers of Au on Pt(100) are probably due to three largely independent effects acting simultaneously. The first effect is an intrinsic bond length change in the monolayer or thin layer relative to the bulk material which may be related to a rehybridization of the bonding orbitals [27]. The second effect is a bond length variation due to electronic interaction between Pt and Au [26]. The third effect is that of the strain in the monolayer or thin layer due to the geometrical misfit with the underlying substrate lattice [28].

The data in table 1 should be able to increase our understanding of these effects.

4.6. The surface structure of platinum on Au(100) at coverages exceeding one monolayer equivalent

Deposition of more than one monolayer equivalent (mle) of platinum onto the Au(100) surface does not change the (1 X 1) pattern that was observed after the first mle. At a coverage of several mle the platinum microcrystallites should coalesce, but LEED did not show any changes in the surface structure up to eight mle, the highest coverage attained in these experiments. Annealing of these surfaces

did not give any new diffraction patterns. However, the platinum on gold system has much less thermal stability than the Au on Pt system. At 520 K, diffusion occurred at such a rate for the Pt on Au system that the Auger signal of the adsorbate became attenuated by 10–15% in a few minutes; in order to induce diffusion of gold into underlying Pt(100) at a similar rate, the crystal had to be heated to 870 K. Since the surface free energy of gold is smaller than that of platinum (1.483 and 2.465 J m^{-2} at 300 K, respectively, calculated with the data from ref. [29]) gold coating of platinum produces a lower total surface free energy system which is therefore more stable. The platinum covered gold system has a higher total surface free energy than the clean gold, leading to a less stable surface. It appears that the difference in the diffusion rates of these two systems reflects the differences in thermodynamic stabilities that are the driving force for change of surface composition of the platinum on gold system, and the stabilizing force for the lower surface free energy gold on platinum system.

5. Appendix

5.1. Determination of the growth mechanisms and electron mean free path lengths of Au on Pt(100) and Pt on Au(100) using AES in combination with the QXTM

Deposited metal atoms can arrange themselves in a number of ways, depending on the adsorbate–adsorbate and adsorbate–substrate interactions. Basically, four different growth mechanisms can be distinguished [30]. One possibility is that the deposited film grows layer-by-layer through the completion of successive full monolayers (Frank–van der Merwe (FM) type growth). On the other hand, the adatoms may aggregate to form three-dimensional islands (microcrystallites) without a preceding monolayer stage (Volmer–Weber (VW) growth mechanism). An intermediate case is the Stranski–Krastanov (SK) type growth where first one monolayer is completed, followed by the growth of three-dimensional islands on top of this monolayer. In the fourth mechanism, surface compound (SC) formation occurs through the formation of a monolayer followed by insertion of substrate atoms in to the adsorbate layer.

As has been discussed in the literature, each growth mechanism gives rise to a different coverage dependence of the adsorbate and substrate Auger signal intensities. Therefore, under conditions of constant deposition rate a plot of the Auger signal versus time (ASt-plot) may identify the growth mechanism of the system under investigation. Ref. [30] gives characteristic examples of ASt-plots for all four growth mechanisms. Briefly, an ASt-plot for the FM growth consists of straight line segments connected by breaks at the completion of every monolayer. The VW growth mechanism gives an ASt-plot with smooth, continuous curves. The buildup of the adsorbate signal and the decrease of the substrate signal intensity are slower than for the FM type growth. The SK mechanism is characterized by straight line

segments from zero to one monolayer connected at the monolayer by breaks to continuous curves at higher coverages. The ASt-plot for SC formation is similar to that of the FM mechanism, but the substrate Auger signal intensity does not vanish at high coverages, nor does the adsorbate signal reach the value of the bulk adsorbate since the surface layer contains both elements.

Quantitative evaluation of the ASt-plots can yield the mean free path of the Auger electrons that are studied [31]. For this purpose the point of deposition of one monolayer or monolayer equivalent has to be known. In those cases where the ASt-plots show breaks, this is easy to determine. Otherwise this cannot be extracted from the Auger data alone. The QXTM can be used to experimentally provide this important information.

5.1.1. Decomposition of the overlapping gold and platinum Auger transitions

The Auger spectra of gold and platinum, which are neighbors in the periodic table, are very similar and give rise to overlapping peaks throughout the entire energyrange. The best resolution of our retarding field analyzer was obtained below 100 eV, where a 2 V peak-to-peak modulation could be used. The region between 45 and 95 eV, where the peak shapes change in a marked way from platinum to gold was chosen for analysis. In this region the Auger electrons are also very surface sensitive since the universal curve of the mean free path of electrons as a function of their energy has its minimum near 60 eV. In this interval of 45–95 eV there are one platinum peak at 64 eV and four gold transitions at 56, 61, 66, and 69 eV. Auger spectra for various coverages of Au on Pt(100) and Pt on Au(100) are shown in figs. 3 and 6, respectively.

Initially it was attempted to perform the peak separation and subsequent analysis using integrated Auger spectra. These can be obtained by numerical integration of the Auger spectra that were recorded in the derivative mode ($dN(E)/dE$). Before integration the background, which depends on both the electron energy and the adsorbate metal coverage, has to be subtracted. However, this background is not known. It can easily be seen that the background increase has to be monotonic and that the areas under the positive and the negative parts of the derivative Auger spectrum from which the background has been subtracted must be equal. These two requirements are, however, not sufficient to determine an unambiguous background. The peak separation could still be carried out using an estimated background that fulfilled these two requirements, but the inaccuracy of the background proved to be a source of scatter in the resulting ASt-plots. For this reason the following peak separation method was devised which eliminates the necessity to know the background of the Auger spectra and further avoids the elaborate integration of spectra that were recorded in the differential mode. This decomposition procedure will be illustrated with the Au on Pt(100) case, see fig. 9. We shall assume that at any given coverage the Auger spectrum is a linear combination of the Auger spectra of pure platinum and pure gold, in this case the clean Pt(100) surface and a thick gold overlayer, respectively.

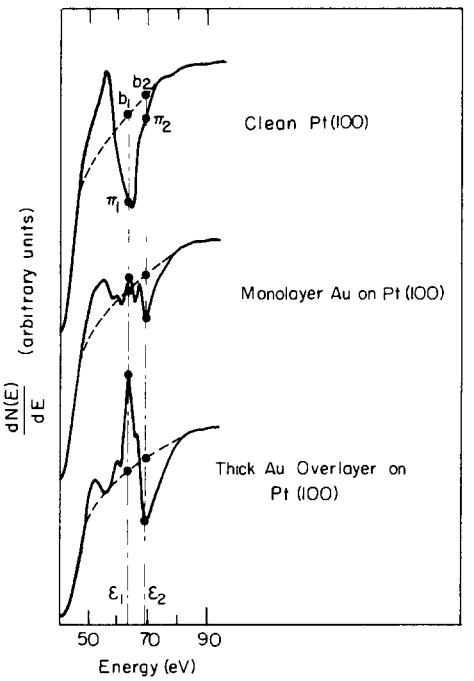

Fig. 9. Illustration of the Auger decomposition for Au on Pt (100).

The Auger signal intensity π is a function of the Auger electron energy ϵ and will be denoted as $\pi^0(\epsilon)$ for the clean substrate, $\pi^\infty(\epsilon)$ for the thick overlayer and $\pi^\theta(\epsilon)$ for a surface with adsorbate coverage θ. The measured signal intensity $\pi(\epsilon)$ has to be corrected for the background $b(\epsilon)$ which is also a function of the energy. Now an arbitrary Auger signal intensity can be written as the linear combination:

$$\pi^\theta(\epsilon) - b^\theta(\epsilon) = f^0[\pi^0(\epsilon) - b^0(\epsilon)] + f^\infty[\pi^\infty(\epsilon) - b^\infty(\epsilon)] \,, \tag{1}$$

where f^0 and f^∞ can be identified as the normalized Auger intensities of platinum and gold after decomposition; they satisfy

$$f^0 + f^\infty = 1 \tag{2}$$

(this relation will be further discussed and justified in section 5.1.2).

Eq. (1) is not useful as it stands since the background $b(\epsilon)$ is not known. This problem can be solved in the following way:

The difference between the signal intensities at two energies ϵ_1 and ϵ_2 is

$$\begin{aligned}\pi^\theta(\epsilon_1) - \pi^\theta(\epsilon_2) - [b^\theta(\epsilon_1) - b^\theta(\epsilon_2)] \\ = f^0\{[\pi^0(\epsilon_1) - \pi^0(\epsilon_2)] - [b^0(\epsilon_1) - b^0(\epsilon_2)]\} \\ + f^\infty\{[\pi^\infty(\epsilon_1) - \pi^\infty(\epsilon_2)] - [b^\infty(\epsilon_1) - b^\infty(\epsilon_2)]\} \,;\end{aligned} \tag{3}$$

f^0 and f^∞ depend on Auger electron energy through the electron mean free path. However, since ϵ_1 and ϵ_2 will be chosen close to each other and both near the minimum of the universal curve, this dependence will be neglected. We shall also assume that the background $b^\theta(\epsilon)$ is a linear combination of $b^0(\epsilon)$ and $b^\infty(\epsilon)$ with the same f^0 and f^∞ as in eq. (1). Now eq. (3) is reduced to

$$\pi^\theta(\epsilon_1) - \pi^\theta(\epsilon_2) = f^0[\pi^0(\epsilon_1) - \pi^0(\epsilon_2)] + f^\infty[\pi^\infty(\epsilon_1) - \pi^\infty(\epsilon_2)] \ . \tag{4}$$

The difference values $\pi(\epsilon_1) - \pi(\epsilon_2)$ are easily measured from the recorded Auger spectra without knowing the background. Eqs. (2) and (4) lead to the desired result:

$$f^\infty = \frac{[\pi^\theta(\epsilon_1) - \pi^\theta(\epsilon_2)] - [\pi^\infty(\epsilon_1) - \pi^\infty(\epsilon_2)]}{[\pi^0(\epsilon_1) - \pi^0(\epsilon_2)] - [\pi^\infty(\epsilon_1) - \pi^\infty(\epsilon_2)]}. \tag{5}$$

In order to obtain accurate results ϵ_1 and ϵ_2 should be chosen such that $\pi(\epsilon_1) - \pi(\epsilon_2)$ shows a strong dependence on the adsorbate coverage. ϵ_1 and ϵ_2 should also be near the minimum of the universal curve, as mentioned before, which led to the choice of $\epsilon_1 = 63$ eV and $\epsilon_2 = 69$ eV.

After separating the gold and platinum contributions in the Auger spectra of Au on Pt(100) (fig. 3), and of Pt on Au(100) (fig. 6), ASt-plots for both systems can be made. Since the deposition rates in both cases were measured with the QXTM prior to deposition onto the actual metal single crystal surfaces, the deposition times can be converted to coverages in terms of monolayer equivalents, which were defined as the ratio of the total number of deposited atoms and the number of substrate surface atoms. The resulting Auger signal versus coverage (ASc) plots are shown in figs. 4 and 7.

5.1.2. Quantitative evaluation of the ASc-plots

In order to treat the data quantitatively, model calculations were made to simulate ASc-plots for the various growth mechanisms and, by optimizing the adjustable parameters, finally, a best fit with the experimental data was obtained.

Since during the decomposition procedure the Auger signal intensities of gold and platinum were evaluated in the same, narrow, energy range near the minimum of the universal curve, equal mean free paths were assumed for the Auger electrons of both elements. As they are neighbors in the periodic table, the relative backscattering coefficient was taken to be unity. The decomposition procedure yields substrate and adsorbate Auger signal intensities, denoted as f^0 and f^∞, that are normalized to the bulk substrate signal and the signal of a thick overlayer, respectively. In the following it will be more convenient to represent these signal intensities in the form of $I(n)/I(\infty)$, where $I(n)$ is the Auger signal intensity of n layers of adsorbate and $I(\infty)$ is the value of the bulk material. The signal from one monolayer of adsorbate, $I(1)/I(\infty)$, is related to the mean free path of the Auger electrons, λ, by

$$I(1)/I(\infty) = 1 - \exp[-d/(0.74\lambda)] \ , \tag{6}$$

where $d = d(h, k, l)$ is equal to the lattice spacing [31]. The factor 0.74 arises as a correction for the acceptance angle of the retarding field analyzer. It follows from eq. (6) and our assumption that the particular Auger electrons of platinum and gold considered here have the same mean free path, that $I(1)/I(\infty)$ is the same for both elements.

Using the Gallon formalism [32] the Auger signal of n monolayers of adsorbate, $I^a(n)/I^a(\infty)$ is now given by

$$I^a(n)/I^a(\infty) = 1 - [1 - I(1)/I(\infty)]^n , \tag{7}$$

while the signal of the substrate covered by these n layers of adsorbate $I^s(n)/I^s(\infty)$, is

$$I^s(n)/I^s(\infty) = [1 - I(1)/I(\infty)]^n . \tag{8}$$

Eqs. (7) and (8) add up to one, which justifies eq. (2) that was used in section 5.1.1. It should be noted that in the general case where the Auger electrons of the adsorbate and substrate have different energies and, consequently, different values of λ and $I(1)/I(\infty)$, eqs. (7) and (8) will not add up to 1. Eqs. 7 and 8 can be used directly to calculate ASc-plots for the FM growth mechanism. For this fit, $I(1)/I(\infty)$ is the only adjustable parameter.

In order to calculate an ASc-plot for the VW type growth, information on the shape of the microcrystallites is necessary. Broad, flat crystallites will give ASc-plots that differ from those of crystallites that are shaped as cylinders. The former will give a relatively stronger coverage dependence of the Auger signal intensities due to a more effective shielding of the substrate and less attenuation of its own Auger electrons, while more cylinder-like crystallites shield less of the substrate and attenuate more of their own Auger electrons that originate in the lower layers of the crystallites, thus yielding a relatively weaker coverage dependence in the ASc-plots. The crystallite shape can be expressed by a distribution function $P(n)$ that gives the fraction of the surface that is covered by exactly n layers of adsorbate at a given nominal coverage of θ monolayer equivalents. We did not attempt to develop a distribution function that accounts in detail for effects of surface free energies and kinetics of diffusion since this requires to many assumptions and parameters that are not known. Instead, the experimental data were fit with two different, relatively simple distribution functions that have either no or only one adjustable parameter, in addition to $I(1)/I(\infty)$. The quality of the fits and the degree of agreement between the parameters resulting from both models can be used as an indication of the sensitivity of the ASc plots to the crystallite shape.

The first model is a simple binomial distribution which can be reduced in this case to the Poisson distribution,

$$P_p(n) = \theta^n e^{-\theta}/n! . \tag{9}$$

Using this model, $I(1)/I(\infty)$ is the only adjustable parameter.

In the second model it is assumed that all crystallites are identical hemispheres.

In order to determine whether the surface is covered by many small islands or fewer, but larger, crystallites, a new adjustable parameter has to be introduced, the concentration of nucleation sites on the surface, C^n. The distribution function $P_H(n)$ for these identical hemispheres is calculated in steps. First, from the nominal coverage θ and C^n the size of the hemispheres is calculated. Then the hemispheres are divided into discrete coaxial cylinders with a height equal to an integer number of layer spacings. The cross-sectional areas of these hollow cylinders with finite wall thickness, expressed as fractional surface areas then give $P_H(n)$. When the coverage is increased, the hemispheres grow until they reach a critical diameter which is equal to the microcrystallite separation where they will touch the surrounding crystallites. Since it is not known what exactly happens at this point, only coverages below this critical point are used for the fitting procedure. With either of these two models, in order to calculate the Auger signal intensity from a surface with a coverage θ, $I(\theta)/I(\infty)$, the surface is divided into parts that are covered by exactly n layers of adsorbate, for all values of n. The Auger signal contribution from each part is given by Eq. (7) or (8), multiplied with the relative surface area of the part that is given by $P(n)$. Thus,

$$I(\theta)/I(\infty) = \sum_{n=0}^{\infty} P(n)\,[I(n)/I(\infty)] \,. \tag{10}$$

The adjustable parameters in fitting the experimental ASc-plots with the VW model are now $I(1)/I(\infty)$ and in one case, C^n.

The modelling of the SK growth involves a combination of the previous two models. At submonolayer coverages the FM model suffices; whereas at coverages above one monolayer the VW model has to be used while at the same time accounting for the first monolayer.

In the case of SC formation the adsorbate signal does not reach the value of the bulk adsorbate material, nor does the substrate signal vanish at high coverages. In the case of Au on Pt(100) and Pt on Au(100) it can be seen from figs. 4 and 7 that this is not the case here and no fitting was attempted.

Acknowledgment

This work was supported by the Director, Office of Energy Research, Office of Basic Energy Sciences, Materials Sciences Division of the US Department of Energy under Contract W-7405-ENG-48.

References

[1] R.L. Jacobsen, H.E. Kluksdahl, C.S. McCoy and R.W. Davis, Preprints API, Division of Refining, 1969, pp. 37–69.

[2] M J Sterba, P C Weinert, A G. Lickus, E L Pollitzer and J.C. Hayes, Oil Gas J 66 (1968) 140.
[3] F.W. Kopf, W.C. Pfefferle, M H. Dalson, W.A. Decker and J A Nevison, Preprints API, Division of Refining, 1969, pp. 23–69.
[4] H.E. Kluksdahl, US Patent 3,415,737 (1968).
[5] C. Betizeau, G. Leclercq, R. Maurel, C. Bolivar, H. Charcosset, R. Frety and L Tournayan, J. Catalysis 45 (1976) 179.
[6] P. Biloen, J.H. Helle, H. Verbeek, F.M. Dautzenberg and W.M.H. Sachtler, J. Catalysis 63 (1980) 112.
[7] B. Spurlock and R L Jacobson, US Patent 3,507,781 (1970).
[8] J.H. Sinfelt, US Patent 3,835,034 (1974).
[9] F.M. Dautzenberg, J.N. Helle, P. Biloen and W.M.H. Sachtler, J Catalysis 63 (1980) 119
[10] J.R.H. Van Schaik, R.P. Dessing and V. Ponec, J. Catalysis 38 (1975) 273.
[11] H.C. De Jongste, F.J. Kuyers and V. Ponec, in Proc. 6th Intern. Congr. on Catalysis, London, 1976, Eds. Bond, Wells and Tompkins, Vol. 2, p B31.
[12] P. Biloen, F.M Dautzenberg and W.M.H Sachtler, J Catalysis 50 (1977) 77
[13] A. O'Cinneide and F.G. Gault, J. Catalysis 37 (1975) 311.
[14] V. Ponec and W.M.H. Sachtler, J. Catalysis 24 (1972) 250.
[15] J.H Sinfelt, J.L Carter and D.J.C. Yates, J Catalysis 24 (1972) 283.
[16] J.P. Bibérian and G.A. Somorjai, J. Vacuum Sci. Technol 16 (1979) 2073.
[17] M.A. Van Hove, R.J. Koestner, P.C. Stair, J.P. Bibérian, L.L Kesmodel, I. Bartos and G.A Somorjai, Surface Sci. 103 (1981) 189, 218.
[18] J.P. Bibérian and G.A. Somorjai, Appl. Surface Sci 2 (1979) 352
[19] F.J. Kuyers, B M Tieman and V. Ponec, Surface Sci 75 (1978) 657
[20] F.J. Kuyers and V. Ponec, Appl. Surface Sci. 2 (1978) 43.
[21] D.G Fedak and N.A. Gjostein, Surface Sci 8 (1967) 77.
[22] P.W. Palmberg and T.N. Rhodin, J. Chem. Phys., 49 (1968) 134.
[23] A. Ignatiev, A.V Jones and T N. Rhodin, Surface Sci. 30 (1972) 573
[24] J. Kuppers and H. Michel, Appl. Surface Sci. 3 (1979) 179;
P. Heimann, J. Hermanson, H. Miosga and H. Neddermeyer, Phys. Rev. Letters 43 (1979) 1757,
J.F. van der Veen, F.J. Himpsel and D.E. Eastman, Phys. Rev. Letters 44 (1980) 189.
[25] P.R. Norton, J.A. Davies, D.P. Jackson and N. Matsunami, Surface Sci. 85 (1979) 269;
D.M. Zehner, B R. Appleton, T.S. Noggle, J W. Miller, J.H. Barrett, L H. Jenkins and O.E. Schow III, J. Vacuum Sci. Technol. 12 (1975) 454.
[26] Handbook of Lattice Spacings and Structures of Metals, Vol. 2, Ed. W.B. Pearson (Pergamon).
[27] L. Brewer, Science 161 (1968) 115.
[28] F.C. Frank and J.H. van der Merwe, Proc Roy. Soc. (London) A189 (1949) 205.
[29] W.R. Tyson, Surface Sci. 62 (1977) 267.
[30] G.E. Rhead, J. Vacuum Sci. Technol. 13 (1976) 603.
[31] M.P. Seah, Surface Sci. 32 (1972) 703.
[32] T.E. Gallon, Surface Sci 17 (1969) 486